Int. J. Heat Mass Transfer. Vol. 19, pp. 385–393. Pergamon Press 1976. Printed in Great Britain

ANALYSIS OF A LAMINAR FLAT PLATE BOUNDARY-LAYER DIFFUSION FLAME

NORBERT PETERS
Institut für Thermo- und Fluiddynamik Technische Universität Berlin, Germany

(*Received* 24 *March* 1975)

Abstract—A numerical analysis of a laminar hydrogen–oxygen diffusion flame in a flat plate boundary layer was carried out in order to investigate its non-equilibrium and close-to-equilibrium structure at various positions in the boundary layer. Variable properties including thermodiffusion and 15 elementary reactions between 8 species were used in the calculation. The results show the ignition and non-equilibrium development of the flame and the approach to local chemical equilibrium within the flame zone. On both sides of the flame zone, due to the low temperatures there, the chemical reactions are practically frozen even at large distances from the leading edge.

NOMENCLATURE

B_{bk},	steric factor of the backward reaction rate coefficient;
B_{fk},	steric factor of the forward reaction rate coefficient;
B_{pk},	pre-exponential factor of the equilibrium constant;
c_i,	mass fraction;
c_i^-,	mass fraction in the injected gas;
c_{pi},	specific heat at constant pressure;
$\bar{c}_p$,	mean specific heat at constant pressure;
D_{ij},	multicomponent diffusion coefficient;
$\mathscr{D}_{ij}$,	binary diffusion coefficient;
D_i^T,	multicomponent coefficient of thermodiffusion;
E_{bk},	activation energy of the backward reaction;
E_{fk},	activation energy of the forward reaction;
E_i,	Eucken factor;
Ec,	Eckert number;
f',	non-dimensional tangential velocity;
H_i,	non-dimensional specific enthalpy;
h_i,	specific enthalpy;
J_i,	non-dimensional diffusion flux;
k_{bk},	backward reaction rate coefficient;
K_{ck},	equilibrium constant in terms of molar densities;
k_{fk},	forward reaction rate coefficient;
K_{pk},	equilibrium constant in terms of partial pressures;
l_0,	Chapman–Rubesin parameter;
Le_{ij},	multicomponent Lewis-number;
Le_i^T,	multicomponent Lewis-number of thermodiffusion;
M,	third body in three-molecular reactions;
M_i,	molecular weight;
$\bar{M}$,	mean molecular weight;
m,	number of species including third bodies;
M_r,	reference molecular weight, = 1 kg/k mol;
n,	number of species;
n_{bk},	exponent of the pre-exponential temperature dependence of the backward reaction;
n_{fk},	exponent of the pre-exponential temperature dependence of the forward reaction;
n_{pk},	exponent of the pre-exponential temperature dependence of the equilibrium constant;
p,	pressure;
Pr,	Prandtl number;
R,	universal gas constant;
r,	number of reactions;
T,	absolute temperature;
T_i^*,	reduced temperature;
u,	tangential velocity;
v,	normal velocity;
V,	non-dimensional normal velocity;
x,	tangential coordinate;
y,	normal coordinate.

Greek symbols

Γ_i,	chemical production rate;
η,	non-dimensional normal coordinate;
θ,	non-dimensional temperature;
λ_i,	thermal conductivity;
$\bar{\lambda}$,	thermal conductivity of the mixture;
μ_i,	dynamic viscosity;
$\bar{\mu}$,	dynamic viscosity of the mixture;
ν'_{jk},	stoichiometric coefficient of the forward reaction;
ν''_{jk},	stoichiometric coefficient of the backward reaction;
ν_{jk},	$\nu''_{jk}-\nu'_{jk}$;
ν'_{ks},	$\sum_{j=1}^{m} \nu'_{jk}$;
ν''_{ks},	$\sum_{j=1}^{m} \nu''_{jk}$;
ν_{ks},	$\nu''_{ks}-\nu'_{ks}$;
ξ,	non-dimensional tangential coordinate;
ρ,	density;
σ_i,	collision cross section.

Subscripts

i, j,	ith or jth species;
k,	kth reaction;
w,	wall;
δ,	boundary-layer edge;
r,	reference state.

1. INTRODUCTION

NEXT to the one-dimensional stagnation point flow, the flat plate boundary layer represents the most generally adopted flow configuration to study boundary layer diffusion flames. Although two-dimensional, the hydrodynamic aspects of the problem are fairly simple and well understood, whereas the interaction of heat and mass transfer with non-equilibrium chemical reactions is rather complex and plays the major part in the analysis. Its practical importance in many modern engineering applications such as combustion chambers, reaction engine nozzles and high temperature heat exchangers is revealed by the great number of experimental and theoretical studies which have been carried out in recent years. Experimental investigations consider the combustion of ethyl alcohol in oxygen [1] and in air [2] as well as the combustion of methane and propane in air [3, 4]. The theoretical works on the problem are generally based on several simplifying assumptions, of which the most important ones are: (1) local similarity of the flow; (2) a single chemical reaction; (3) neglection of the reverse reactions and (4) local chemical equilibrium.

The assumptions (2), (3) and (4) may be summarized to give: (5) the flame sheet model.

Theoretical investigations of laminar flat plate boundary layer diffusion flames based on the assumptions (1) and (5) are reported in [1, 2] and [5–9]. Recently, a numerical analysis based on the assumptions (2) and (3) was reported, which considered the non-equilibrium features of the flow [10].

In flat plate chemically reacting boundary layers, the local Damköhler number is based on the distance from the leading edge as appropriate reference length. Consequently, the local Damköhler numbers may grow from zero at the leading edge to very high values at positions far downstream. The local equilibrium is attained when the Damköhler numbers of the fastest independent reactions asymptotically approach infinity [11]. An asymptotic expansion of the system of governing equations in terms of high Damköhler numbers shows that this limit is singular. Related to this singularity, the numerical solution of the governing equations becomes extremely difficult [12–15] in close-to-equilibrium flows, whereas the equilibrium solution based on the law of mass action is relatively easy to obtain.

In the present paper the development of a hydrogen–oxygen diffusion flame running through the stages of mixing, ignition and non-equilibrium combustion to reach the close-to-equilibrium combustion state far downstream of the leading edge is analysed numerically. Behind an impermeable leading section of 0·15 cm, gaseous hydrogen is injected at a constant rate into the oncoming oxygen stream (Fig. 1). The leading section is assumed to be highly heated in order to allow ignition to occur. Rather than to assume a single overall reaction, a set of 15 elementary reactions between the species H, H_2, O, OH, H_2O, O_2, HO_2 and H_2O_2 is used in the calculation. To obtain a realistic picture of the mixing and ignition process, multicomponent

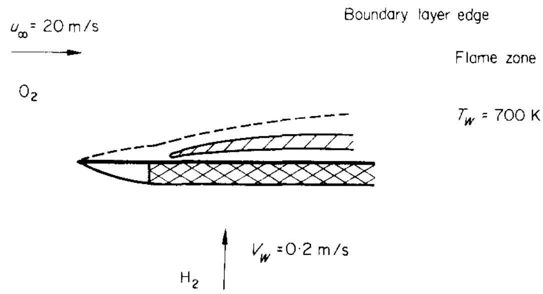

FIG. 1. Flow configuration.

diffusion as well as thermodiffusion is included in the analysis. The non-similar characteristics of the flow are followed from the leading edge to a downstream position, where the flame is fully established and the profiles of velocity, temperature and concentrations become nearly similar.

2. GOVERNING EQUATIONS

The set of r elementary gas phase reactions occurring in the n component system is given by the reaction equations

$$\sum_{j=1}^{m} \nu'_{jk} X_j \rightleftarrows \sum_{j=1}^{m} \nu''_{jk} X_j \quad (k = 1, 2, \ldots, r). \tag{1}$$

The boundary-layer flow of a chemically reacting gas mixture over a flat plate with zero pressure gradient is described by the boundary layer equations. Using the similarity variables

$$\xi = (\rho\mu)_\delta u_\delta x \tag{2}$$

$$\eta = \frac{u_\delta}{\sqrt{(2\xi)}} \int_0^y \rho \, dy \tag{3}$$

these take the non-dimensional form [16, 17]:
continuity

$$2\xi \frac{\partial f'}{\partial \xi} + \frac{\partial V}{\partial \eta} + f' = 0 \tag{4}$$

momentum

$$2\xi f' \frac{\partial f'}{\partial \xi} + V \frac{\partial f'}{\partial \eta} = \frac{\partial}{\partial \eta}\left(l_0 \frac{\partial f'}{\partial \eta}\right) \tag{5}$$

energy

$$2\xi f' \frac{\partial \theta}{\partial \eta} + V \frac{\partial \theta}{\partial \eta} = \frac{1}{\bar{c}_p} \frac{\partial}{\partial \eta}\left(\frac{l_0 \bar{c}_p}{Pr} \frac{\partial \theta}{\partial \eta}\right) - \sum_{i=1}^{n} \left(\frac{c_{pi}}{\bar{c}_p} J_i \frac{\partial \theta}{\partial \eta} + H_i \Gamma_i\right) + Ecl_0 \left(\frac{\partial f'}{\partial \eta}\right)^2 \tag{6}$$

concentration

$$2\xi f' \frac{\partial c_i}{\partial \xi} + V \frac{\partial c_i}{\partial \eta} = -\frac{\partial J_i}{\partial \eta} + \Gamma_i \quad (i = 1, 2, \ldots, n). \tag{7}$$

In these equations, the following non-dimensional quantities have been introduced:
tangential velocity

$$f' = \frac{u}{u_\delta} \tag{8}$$

normal velocity

$$V = \frac{2\xi}{(\rho\mu)_\delta u_\delta}\left(f'\frac{\partial\eta}{\partial x} + \frac{\rho v}{\sqrt{(2\xi)}}\right) \quad (9)$$

temperature

$$\theta = \frac{T}{T_r} \quad (10)$$

enthalpy

$$H_i = \frac{h_i}{\bar{c}_p T_r} \quad (11)$$

diffusion flux

$$J_i = \frac{l_0}{Pr}\left\{\frac{M_i}{\overline{M}^2}\sum_{\substack{k=1\\ i\neq k}}^{n} Le_{ik}\frac{\partial}{\partial\eta}(\overline{M}c_k) - \frac{Le_i^T}{\theta}\frac{\partial\theta}{\partial\eta}\right\} \quad (12)$$

chemical production rate of the species

$$\Gamma_i = \frac{M_i}{M_r}\sum_{k=1}^{r} \nu_{ik} Da_{fk} S_k \quad (13)$$

where the quantity S_k is defined

$$S_k = \left(\frac{M_r}{\rho}\right)^{\nu_{ks}}\left\{\sum_{j=1}^{m}\left(\frac{\rho c_i}{M_j}\right)^{\nu'_{jk}} - \frac{1}{K_c(T)}\sum_{j=1}^{m}\left(\frac{\rho c_i}{M_j}\right)^{\nu''_{jk}}\right\}. \quad (14)$$

The mean specific heat and mean molecular weight in these equations are

$$\bar{c}_p = \sum_{i=1}^{n} c_i c_{pi} \quad (15)$$

$$\overline{M} = \left(\sum_{i=1}^{n}\frac{c_i}{M_i}\right)^{-1}. \quad (16)$$

The non-dimensional similarity parameters are defined: Chapman–Rubesin-parameter

$$l_0 = \frac{\rho\bar{\mu}}{(\rho\mu)_\delta}, \quad (17)$$

Prandtl number

$$Pr = \frac{\bar{\mu}\bar{c}_p}{\bar{\lambda}}, \quad (18)$$

Eckert number

$$Ec = \frac{u_\delta^2}{\bar{c}_p T_r}, \quad (19)$$

Lewis number

$$Le_{ik} = \frac{\rho D_{ik}\bar{c}_p}{\bar{\lambda}}, \quad (20)$$

Lewis number of thermodiffusion

$$Le_i^T = \frac{D_i^T\bar{c}_p}{\bar{\lambda}}, \quad (21)$$

First local Damköhler number

$$Da_{fk} = \frac{2B_{fk}T_r^{n_{fk}}\mathrm{e}^{-\beta_{fk}}}{u_\delta/L} \times\left(\frac{\rho_r}{M_r}\right)^{\nu_{ks}-1}\left(\frac{x}{L}\right)\theta^{n_{fk}}\mathrm{e}^{-\beta_{fk}\left(\frac{1}{\theta}-1\right)}. \quad (22)$$

Non-dimensional activation energy

$$\beta_{fk} = \frac{E_{fk}}{RT_r}. \quad (23)$$

Finally, the equation of state of an ideal gas mixture is given by

$$p_\delta = \rho\frac{R}{\overline{M}}T. \quad (24)$$

The boundary conditions of the differential equations (4)–(7) are as follows

$\eta = 0$:

$$V = \rho v_w(x)\sqrt{\left(\frac{2x}{(\rho\mu)_\delta u_\delta}\right)} \quad (25)$$

$$f' = 0 \quad (26)$$

$$\theta = \frac{T_w(x)}{T_r} \quad (27)$$

$$J_i + V(c_i - c_i^-) = 0 \quad (28)$$

$\eta = \eta_\delta$:

$$f' = 1 \quad (29)$$

$$\theta = \frac{T_\delta}{T_r} \quad (30)$$

$$c_i = c_{i\delta}. \quad (31)$$

In the heterogeneous mass balance at the wall, equation (28), c_i^- denotes the concentration of the injected gas. Heterogeneous reactions have been neglected for simplicity. The initial conditions at the leading edge are determined by substituting $\xi = 0$ into the equations (4)–(8), and solving the resulting ordinary differential equations numerically.

3. NUMERICAL CALCULATIONS AND PROPERTIES

The above system of differential equations was solved using an implicit fourth order Hermitian finite difference method described in [18] and [19]. The main difficulty in solving the resulting difference equations consisted in linearizing the chemical production rate. It was found that at large Damköhler numbers only a Newton–Raphson iteration technique was able to give satisfactory results. The higher order accuracy of the Hermitian finite difference method allowed to reduce the number of grid points to as few as 26 across the boundary layer between $\eta = 0$ and $\eta_\delta = 5{\cdot}0$. The step size in flow direction was varied continuously so that not more than 2 iterations were required at each position. Thus very small steps were to be taken during the ignition period and at large distances from the leading edge where local equilibrium was approached.

The following auxiliary relations were used to calculate the non-constant properties of the system: The specific enthalpy is defined

$$h_i = h_i^+ + \int_{T^+}^{T} c_{pi}\,\mathrm{d}T \quad (32)$$

where h_i^+ is the reference enthalpy at $T^+ = 298{\cdot}15$K. The specific heat c_{pi} is approximated from [20] by

$$c_{pi} = A_i + B_i \ln T + C_i T^{-1} + D_i T^{-2}. \quad (33)$$

Table 1

	H	H_2	O	OH
M_i(kmol/kg)	1·008	2·016	16·000	17·008
h_{im}^+(kcal/mol)	52·1	0·0	59·56	9·290
π_{iA}(kcal/mol)	3·416	−0·2526	8·835	6·217
π_{iB}(kcal/mol ln k)	1·735	2·618	1·763	2·642
A_i(cal/mal)	4·968	−9·772	0·8094	0·3987
B_i(cal/mol ln K)	0·0	2·256	4·962	1·048
C_i(cal K/mol) . 10^{-2}	0·0	16·47	8·198	−3·133
D_i(cal K^2/mol) . 10^{-4}	0·0	−15·15	−10·30	16·61
σ_i(Å)	2·708	2·827	3·050	3·147
$(\varepsilon/k)_i$(K)	37·0	59·7	106·7	79·8
	H_2O	O_2	HO_2	H_2O_2
M_i(kmol/kg)	18·016	32·000	33·008	34·016
h_{im}^+(kcal/mol)	−57·80	0·0	5·00	−32·53
π_{iA}(kcal/mol)	1·487	7·431	4·188	8·956
π_{iB}(kcal/mol ln k)	3·508	2·865	3·839	3·238
A_i(cal/mol)	1·699	1·053	16·24	−2·507
B_i(cal/mol ln K)	1·534	1·072	−0·2046	0·2631
C_i(cal K/mol) . 10^{-2}	−27·16	−2·583	−39·24	−6·136
D_i(cal K^2/mol) . 10^{-4}	59·92	6·404	57·23	−1·061
σ_i(Å)	2·641	3·467	3·517	4·196
$(\varepsilon/k)_i$(K)	809·1	106·7	79·5	289·3
	A_j	B_j	C_j	D_j
$\ln\Omega^{(1,1)}$	0·021414	−0·122085	0·505088	−0·074757
$\ln\Omega^{(2,2)}$	−0·042775	−0·13594	0·460717	−0·061149

The constants A_i, B_i, C_i and D_i and h_i^+ are given in Table 1. The viscosity and the thermal conductivity of the mixture are [21, 22]

$$\bar{\mu} = \sum_{i=1}^{n} \frac{c_i \mu_i}{M_i \delta_i} \tag{34}$$

$$\bar{\lambda} = \sum_{i=1}^{n} \frac{c_i \lambda_i}{M_i \delta_i} \tag{35}$$

where

$$\mu_i = 2{\cdot}6693 \,.\, 10^{-5} \frac{(M_i T)^{1/2}}{\sigma_i^2 \Omega^{(2,2)}(T_i^*)} \tag{36}$$

$$\lambda_i = 3{\cdot}75 \mu_i \frac{R}{M_i} E_i \tag{37}$$

$$\delta_i = \frac{c_i}{M_i} + \sum_{\substack{k=1\\k\neq i}}^{n} G_{ik} \frac{c_k}{M_k} \tag{38}$$

$$G_{ik} = \frac{1}{\sqrt{8}} \left\{1 + \frac{M_i}{M_k}\right\}^{-1/2} \left\{1 + \left(\frac{\mu_i}{\mu_k}\right)^{1/2} \left(\frac{M_k}{M_i}\right)^{1/4}\right\}^2. \tag{39}$$

The Eucken factor E_i is evaluated by [23]:

$$E_i = 0{\cdot}115 + 0{\cdot}534 \frac{M_i c_{pi}}{R}. \tag{40}$$

The binary diffusion coefficient is given by

$$\mathscr{D}_{ij} = \frac{0{\cdot}0018583 \,.\, T^{3/2}(M_i + M_j)^{1/2}(M_i M_j)^{-1/2}}{p \sigma_{ij}^2 \Omega^{(1,2)}(T_{ij}^*)}. \tag{41}$$

The Lennard Jones collision integrals in (36) and (41) were approximated to a maximum error of 2·5 per cent (see Table 1) by

$$\ln \Omega^{(i,j)} = A_j + B_j \ln T^* + C_j \ln T^{*-1} + D_j T^{*-2}. \tag{42}$$

The reduced temperature in these formulas is defined

$$T_i^* = \frac{T}{(\varepsilon/k)_i} \quad \text{or} \quad T_{ij}^* = \frac{T}{(\varepsilon/k)_{ij}} \tag{43}$$

with

$$(\varepsilon/k)_{ij} = \{(\varepsilon/k)_i (\varepsilon/k)_j\}^{1/2}. \tag{44}$$

The collision cross section σ_{ij} to calculate the binary diffusion coefficient is given by

$$\sigma_{ij} = \frac{\sigma_i + \sigma_j}{2}. \tag{45}$$

Values for σ_i and $(\varepsilon/k)_i$ from [24] are listed in Table 1. From equations (36) and (41) μ_i is obtained in g/cm s and $\mathscr{D}_{ij}$ in cm^2/s, if one introduces T in K, σ in Å and p in atm [21]. The multicomponent diffusion coefficients D_{ij} may be obtained by inversion of a matrix with the following coefficients [17]

$$A_{ij} = \frac{c_i}{\mathscr{D}_{ij}} + \sum_{\substack{k=1\\k\neq i}}^{n} \frac{M_j c_k}{M_k \mathscr{D}_{ik}} \quad (i \neq j) \tag{46}$$

$$A_{ii} = 0.$$

If the elements of the inverted matrix of A_{ij} are denoted by A_{ij}^{-1} this leads to

$$D_{ij} = A_{ij}^{-1} - \frac{M_i}{M_j} A_{ii}^{-1}. \tag{47}$$

The multicomponent coefficient of thermodiffusion is calculated from the equation in [25] by

$$D_i^T = \frac{1}{R} \sum_{\substack{k=1\\k=1}}^{n} c_i c_k \frac{M_i M_k}{M_i + M_k} (\tfrac{6}{5} C_{ik}^* - 1) . \left\{\frac{\lambda_k}{M_k \delta_k} - \frac{\lambda_i}{M_i \delta_i}\right\} \tag{48}$$

Table 2

Reaction	B_{fk} (m^3/kmol s)	n_{fk}	E_{fk}/R (°K)	Ref.
1. $O_2+H \to O+OH$	$2 \cdot 2 . 10^{11}$	0·0	8400·0	[29]
2. $H_2+O \to H+OH$	$1 \cdot 7 . 10^{10}$	0·0	4775·0	[28]
3. $H_2O+H \to H_2+OH$	$8 \cdot 4 . 10^{10}$	0·0	10050·0	[28]
4. $OH+OH \to H_2O+O$	$5 \cdot 8 . 10^{9}$	0·0	390·0	[28]
5. $OH+OH \to H+HO_2$	$1 \cdot 2 . 10^{10}$	0·0	20200·0	[27]
6. $H_2+O_2 \to H+HO_2$	$5 \cdot 5 . 10^{10}$	0·0	29100·0	[27]
7. $HO_2+HO_2 \to H_2O_2+O_2$	$2 \cdot 0 . 10^{9}$	0·0	0·0	[27]
8. $H_2O_2+OH \to H_2O+HO_2$	$1 \cdot 0 . 10^{10}$	0·0	900·0	[29]
9. $H_2O_2+H \to H_2+HO_2$	$2 \cdot 3 . 10^{10}$	0·0	4600·0	[29]
10. $H_2O_2+H \to H_2O+OH$	$3 \cdot 2 . 10^{11}$	0·0	4500·0	[29]
11. $H_2+M \to H+H+M$	$2 \cdot 2 . 10^{11}$	0·0	48300·0	[27]
12. $H_2O+M \to H+OH+M$	$2 \cdot 2 . 10^{13}$	0·0	52900·0	[27]
13. $H_2O_2+M \to OH+OH+M$	$1 \cdot 2 . 10^{14}$	0·0	22900·0	[29]
14. $HO_2+M \to O_2+H+M$	$2 \cdot 4 . 10^{12}$	0·0	23950·0	[29]
15. $O_2+M \to O+O+M$	$2 \cdot 5 . 10^{13}$	0·5	59300·0	[30]

where C_{ik}^{*} is set constant equal to 0·93 as a compromise between experimental [26] and theoretical values [22] for C_{ik}^{*}.

The reaction rate coefficient is approximated by

$$k_{fk}(T) = B_{fk}\, T^{n_{fk}} \exp\left\{-\frac{E_{fk}}{RT}\right\}. \quad (49)$$

The required constants for the 15 reactions used in the calculation are taken from [27–30] and are given in Table 2. The equilibrium constant is

$$K_{ck}(T) = \frac{K_{pk}(T)}{(RT)^{\nu_{ks}}}. \quad (50)$$

To evaluate $K_{pk}(T)$ from the given thermodynamic data, the quantity

$$\pi_i^0 = \frac{(h_i^+ - g_i^0)M_i}{T} \quad (51)$$

has been approximated from [20] (see Table 1) by

$$\frac{\pi_i^0}{R} = \pi_{iA} + \pi_{iB} \ln T. \quad (52)$$

This leads to

$$K_{pk}(T) = B_{pk}\, T^{n_{pk}} \exp\left\{-\frac{\Delta H_k}{RT}\right\} \quad (53)$$

with

$$B_{pk} = \exp \sum_{i=1}^{n} \nu_{ik} \pi_{iA} \quad (54)$$

$$n_{pk} = \sum_{i=1}^{n} \nu_{ik} \pi_{iB} \quad (55)$$

$$\Delta H_k = \sum_{i=1}^{n} \nu_{ik} h_i^+ M_i. \quad (56)$$

Since (53) has the same form as (49), the reaction rate coefficients of the backward reactions takes the form

$$k_{bk}(T) = \frac{k_{fk}(T)}{K_{ck}(T)} = B_{bk}\, T^{n_{bk}} \exp\left\{-\frac{E_{bk}}{RT}\right\}. \quad (57)$$

The calculation was carried out using the following values at the boundaries

$$v_w(x) = \begin{cases} 0 & \text{for} \quad x \leqslant x_0 \\ 0 \cdot 2\,\text{m/s} & \quad x \leqslant x_0 \end{cases}$$

$$T_w(x) = \begin{cases} 2800\text{K} & \text{for} \quad x \leqslant \dfrac{x_0}{2} \\ \text{linear between 2800K and 700K} & \text{for} \quad \dfrac{x_0}{2} < x \leqslant x_0 \\ 700\text{K} & \quad x > x_0 \end{cases}$$

$$u_\delta = 20\,\text{m/s}$$

$$T_\delta = 300\text{K}$$

$$c_{i\delta} = \begin{cases} 1 & i = O_2 \\ 0 & i = H, H_2, O, OH, H_2O, HO_2, H_2O_2 \end{cases}$$

$$c_i^- = \begin{cases} 1 & i = H_2 \\ 0 & i = H, O, OH, H_2O, O_2, HO_2, H_2O_2. \end{cases}$$

4. RESULTS AND DISCUSSION

The results of the numerical calculation are plotted over the boundary layer coordinate η in the Figs. 2–8. The velocity profile (Fig. 2), although quite different from the Blasius profile, is very little affected by the development of the flame and stays nearly similar. The oncoming oxygen dissociates during the flow over the highly heated leading section generating atomic oxygen concentrations up to $c_O = 7 \cdot 5 . 10^{-5}$ close to the wall. When the oxygen mixes with the injected hydrogen right behind the leading section, the reaction mechanism in initiated. Starting mainly with reaction 2 (Table 2) and partly with reaction 6, H, OH and HO_2 radicals are formed. Branching reactions, such as reaction 1 in combination with reaction 2, produce further radicals. When final products such as H_2O and H_2O_2 are formed by radical recombination, heat is released and the ignition process speeds up.

In Fig. 3 the temperature profile is shown at $x = 0 \cdot 155$, 0·166, 0·168 and 0·568 cm. There is only a slight increase in temperature between $x = 0 \cdot 155$ and 0·166 cm corresponding to the induction period where

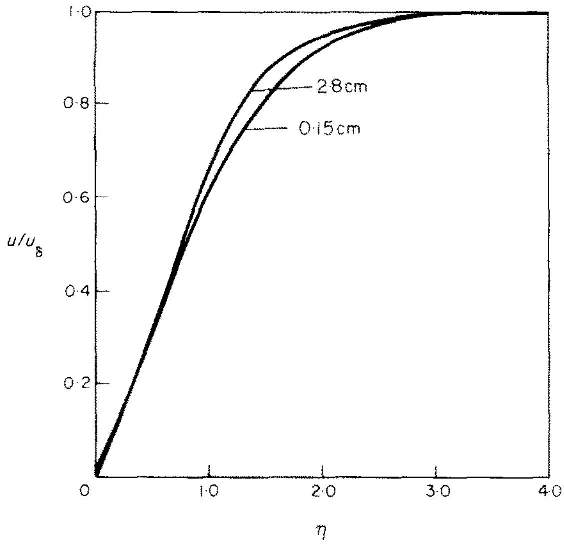

FIG. 2. Velocity profiles.

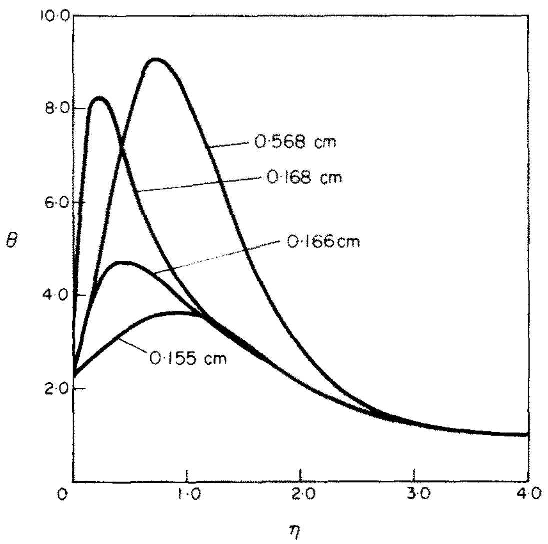

FIG. 3. Temperature profiles.

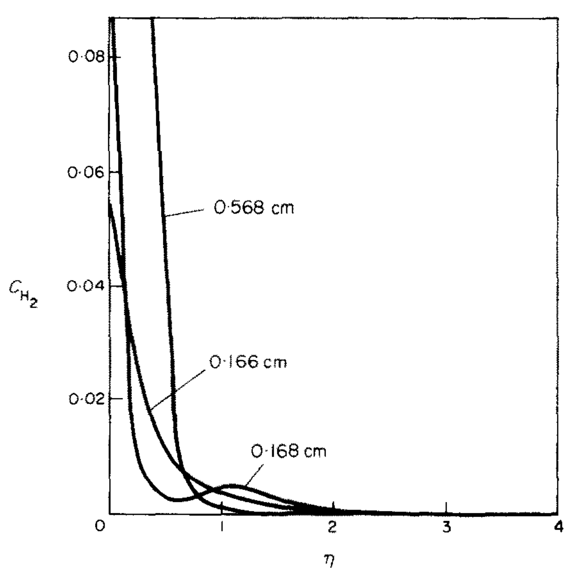

FIG. 4. Molecular hydrogen profiles.

mainly radicals are formed. Between 0·166 and 0·168 cm though, i.e. within 20 μm or 1 μs (based on the free stream velocity), a very sharp rise of the temperature maximum is observed close to the wall. The corresponding concentration profiles of H_2, O_2 and H_2O are shown in the Figs. 4–6 respectively. From Fig. 4 it is seen, that at $x = 0{\cdot}166$ the hydrogen is mainly transported by convection and diffusion and is not yet affected by chemical reactions. At $x = 0{\cdot}168$ cm though, a rapid consumption of H_2 is observed close to the wall, where a local minimum in the H_2-profile appears. Ignition has taken place, but the diffusion flame has not yet reached the region $\eta > 1$ where a higher hydrogen concentration is maintained. As the flow moves on, due to heat conduction and convection, a weak deflagration wave travels across the boundary layer, displacing the temperature maximum to higher values of η and consuming the hydrogen on the right of the flame front totally (Figs. 3 and 4). At the same time all the oxygen on the left side of the flame front is consumed and H_2O is produced in the diffusion flame (Figs. 5 and 6).

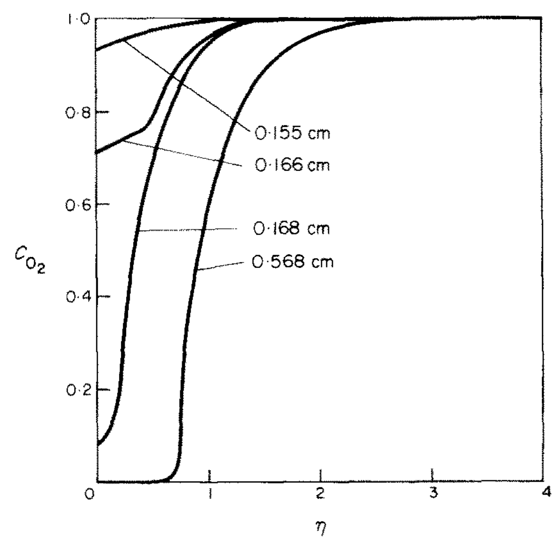

FIG. 5. Molecular oxygen profiles.

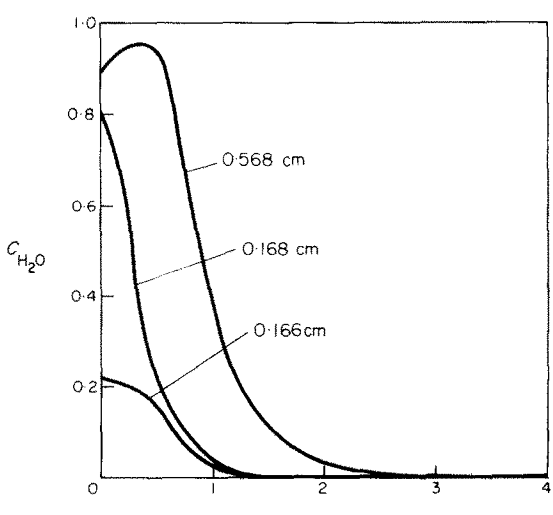

FIG. 6. Water vapour profiles.

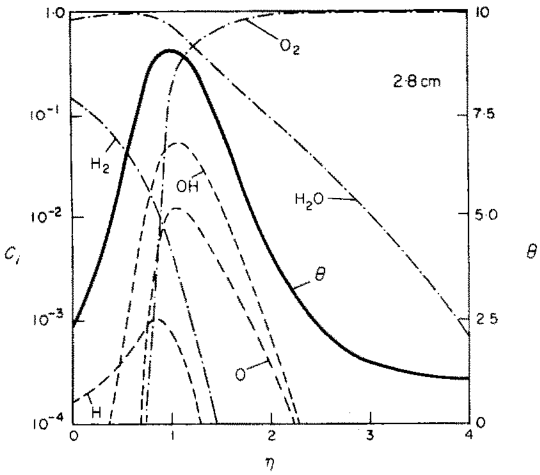

FIG. 7. Downstream solution.

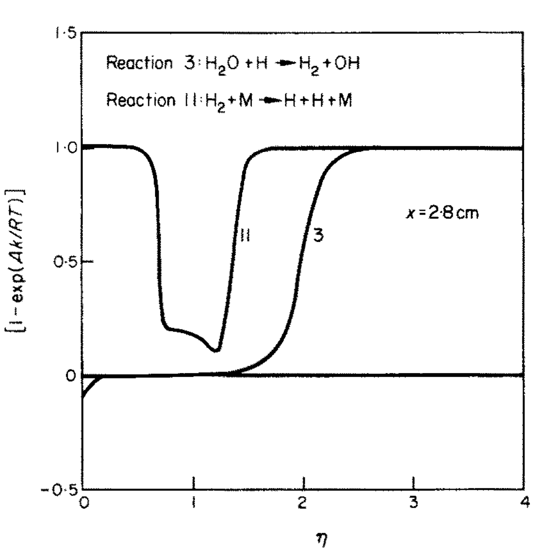

FIG. 8. Approach to local chemical equilibrium.

In Fig. 7 a logarithmic scale is used to plot the concentrations of H, H_2O, OH, O_2 and H_2O along with the temperature over η at 2·8 cm from the leading edge. The values of the concentrations of HO_2 and H_2O_2 were less than 10^{-4} and are not shown in this diagram. It is seen from Fig. 7 that a rather broad flame front appears within the boundary layer at $\eta = 1$ with a maximum temperature corresponding to about 2700K. The OH and O concentration profiles have their peak at the same position as the temperature profile while the maximum of the H-radical profile is shifted to the left. Molecular hydrogen and oxygen diffuses across the flame front and the profiles cross each other at a value of 10^{-2} close to $\eta = 1$.

Due to the high temperature within the flame front, the reaction velocities are very high and local equilibrium is approached locally. This was verified by calculating locally the affinities A_k of the 15 reactions considered

$$A_k = -RT \ln K_{ck} + RT \sum_{j=1}^{n} v_{jk} \, . \ln\left(\frac{\rho c_j}{M_j}\right). \quad (58)$$

With this definition, the quantity S_k, equation (14) becomes

$$S_k = \prod_{j=1}^{n} \left(\frac{\rho c_j}{M_j/M_r}\right)^{v'_{jk}} \left\{1 - \exp\left(\frac{A_k}{RT}\right)\right\}. \quad (59)$$

Rather than A_k itself, the quantity

$$D_k = 1 - \exp\left(\frac{A_k}{RT}\right) \quad (60)$$

which appears in the brackets on the RHS of (59) and thus in the concentration equation, has been plotted over η for two typical reactions, the reaction 3 and the reaction 11, in Fig. 8. At large values of the equilibrium constant and low concentrations of the species on the RHS of the reaction equation, the affinities take large negative values. Thus the quantity D_k approaches unity. On the other hand, as the local chemical equilibrium is approached, the affinity must vanish and D_k approaches zero. It is seen from Fig. 8, that the value of D_{11} is unity everywhere in the boundary layer except for a small region around $\eta = 1$, where it takes values of about 0·15. Thus, the reaction is far from chemical equilibrium on both sides of the flame and close to equilibrium in the flame front. The value of D_3 which is unity in the outer region, remains zero between $\eta = 0·2$–$1·5$, and changes its sign for $\eta < 0·2$ close to the wall. Here A_k obviously becomes positive due to the injected hydrogen. The region of local chemical equilibrium of this reaction is much larger than that of reaction 11.

5. CONCLUSIONS

There are several stages in the development of a hydrogen–oxygen diffusion flame, which have been revealed by a non-equilibrium computation: The mixing, ignition and the non-equilibrium and close-to-equilibrium combustion. The approximation assuming boundary layer similarity is valid only at a relatively large distance from the leading edge, where the diffusion flame is fully developed. In this region there appears a broad flame zone with relatively high radical concentrations. Within the flame zone, the local chemical equilibrium is gradually approached, while outside of it the flow is practically frozen. This confirms the physical reasoning of Libby and Economos [31], who proposed a "flame zone model" based on local chemical equilibrium in the flame zone and frozen flow outside.

Mathematically, this model is justified in the limit of very large activation energies. The exponential temperature dependence of the local Damköhler number has the limit

$$\lim_{\beta_{fk} \to \infty} e^{-\beta_{fk}\left(\frac{1}{\theta} - 1\right)} = \begin{cases} \infty & \text{for } \theta > 1 \\ 1 & \text{for } \theta = 1 \\ 0 & \text{for } \theta < 1. \end{cases} \quad (61)$$

If one assumes a value of $T_r = 1000°K$ for the reference temperature, it may be seen from Table 2 that the non-dimensional activation energies of most of the reactions take large values. Consequently, as the local Damköhler numbers tend to infinity within the region $T > T_r$ in view of the limit (16), the local chemical equilibrium is approached there. On the other hand, the flow is chemically frozen in the region $T < T_r$ as the local Damköhler numbers tend to zero. This behaviour is well illustrated by the shape of D_k in Fig. 8.

REFERENCES

1. G. T. Sergeev, B. M. Smolsky and L. I. Tarsevich, Heat and mass transfer for reaction of injected fluid with external oxygen flow, *Int. J. Heat Mass Transfer* **13**, 1215–1224 (1970).
2. Y. Nakagawa, N. Nishiwaki and M. Hirata, Effect of combustion on a laminar boundary layer, in *13th Symposium (International) on Combustion*, pp. 813–819. The Combustion Institute, Pittsburgh (1971).
3. V. M. Yeroshenko, A. L. Yermakov, A. A. Klimov, V. P. Motulevich and Yu. N. Terent'yev, Investigation of the laminar boundary layer at a permeable surface, *Heat Transfer–Soviet Res.* **5**, 52–56 (1973).
4. T. Hirano and Y. Kanno, Aerodynamic and thermal structures of the laminar boundary layer over a flat plate with a diffusion flame, *14th Symposium (International) on Combustion*, pp. 391–398. The Combustion Institute, Pittsburgh (1973).
5. H. W. Emmons, Film combustion of liquid fuels, *Z. Angew. Math. Mech.* **36**, 60–70 (1956).
6. A. Q. Eschenroeder, Combustion in the boundary layer on a porous surface, *J. Aerospace Sci.* **27**, 901–906 (1960).
7. T. Chen and T. Toong, Laminar boundary layer wedge flows with evaporation and combustion, in *Heterogeneous Combustion Process in Astronautics and Aeronautics* Vol. 15, pp. 643–664. Academic Press, New York (1964).
8. P. A. Libby and M. Pierucci, Laminar boundary layer with hydrogen injection including multicomponent diffusion, *AIAA Jl* **2**, 2118–2126 (1964).
9. H. Krier and H. Kerzner, Analysis of the chemically reacting laminar boundary layer during hybrid combustion, *AIAA Jl* **11**, 1691–1697 (1973).
10. S. Kikkawa and K. Yoshikawa, Theoretical investigation on laminar boundary layer with combustion on a flat plate, *Int. J. Heat Mass Transfer* **16**, 1215–1229 (1973).
11. N. Peters, Strömungen reagierender Gase in der Nähe des chemischen Gleichgewichts, Habilitationsschrift, Technische Universität Berlin (1975).
12. F. A. Fay and H. Kaye, A finite-difference solution of similar nonequilibrium boundary layers, *AIAA Jl* **5**, 1949–1954 (1967).
13. C. Scaccia and L. A. Kennedy, Calculating two-dimensional chemically reacting flows, *AIAA Jl* **12**, 1268–1272 (1974).
14. G. Emmanuel, Problems underlying the numerical integration of chemically and vibrating rate equations in a nonequilibrium flow, AEDC Rept. TDR-63-82, Arnold Engineering Development Center, Tullahoma, Tenn. (1963).
15. C. P. Li, Hypersonic nonequilibrium flow past a sphere at low Reynolds numbers, AIAA Paper 74-173, Washington D.C. (1974).
16. P. M. Chung, Chemically reacting nonequilibrium boundary layers, *Adv. Heat Transfer* **2**, 109–270 (1965).
17. F. G. Blottner, Finite-difference methods of solution of the boundary layer equations, *AIAA Jl* **8**, 193–205 (1970).
18. N. Peters, Boundary layer calculations by a hermitian, finite difference method, Proceedings of the Fourth International Conference on Numerical Methods in Fluid Dynamics, Boulder, Colorado, to appear in Lecture Notes on Physics.
19. N. Peters, Lösung der Grenzschichtgleichungen für chemisch reagierende Gase mit einem Mehrstellenverfahren, Deutsche Luft- und Raumfahrt, DLR-FB 72-58 (1972).
20. D. R. Stull, JANAF-Thermochemical tables, US Department of Commerce (1971).
21. R. B. Bird, W. E. Stewart and E. N. Lightfoot, Transport Phenomena, pp. 24, 258, 571. John Wiley, New York (1960).
22. J. O. Hirschfelder, C. F. Curtiss and R. B. Bird, *Molecular Theory of Gases and Liquids*, pp. 528–539. John Wiley, New York (1964).
23. E. A. Mason and S. C. Saxena, Approximate formula for the thermal conductivity of gas mixtures, *Physics Fluids* **1**, 361–369 (1958).
24. R. A. Svehla, Estimated viscosities and thermal conductivities of gases at high temperatures, NASA TR R-132 (1962).
25. D. Straub, Die polynären Thermodiffusionskoeffizienten von Gasgemischen, *Wärme- und Stoffübertragung* **3**, 211–219 (1971).
26. K. S. Yun and E. A. Mason, Collision integrals for the transport properties of dissociating air at high temperatures, *Physics Fluids* **5**, 380–386 (1962).
27. D. L. Baulch, D. D. Drysdale, D. G. Horne and A. C. Lloyd, *Evaluated Kinetic Data for High Temperature Reactions*, Vol. 1. Butterworth, London (1972).
28. D. L. Baulch, D. D. Drysdale and A. C. Lloyd, High temperature reaction rate data report No. 2, The University, Leeds 2, England (1968).
29. D. L. Baulch, D. D. Drysdale and A. C. Lloyd, High temperature reaction rate data report No. 3, The University, Leeds 2, England (1969).
30. K. L. Wray, Kinetics of O_2 dissociation and recombination, in *10th Symposium (International) on Combustion*, pp. 523–537. The Combustion Institute, Pittsburgh (1965).
31. P. A. Libby and C. Economos, A flame zone model for chemical reaction in a laminar boundary layer with application to the injection of hydrogen–oxygen mixtures, *Int. J. Heat Mass Transfer* **6**, 113–128 (1963).

ETUDE D'UNE FLAMME LAMINAIRE DE DIFFUSION DANS UNE COUCHE LIMITE SUR UNE PLAQUE PLANE

Résumé—Le calcul numérique d'une flamme laminaire de diffusion entre hydrogène et oxygène fut executé dans le but d'examiner sa structure dans le domaine de non-équilibre et dans l'approximité de l'équilibre à des lieux divers de la couche limite. Le calcul tient compte des propriétés de matière variables, la thermodiffusion incluse, et de 15 réactions élémentaires entre 8 composants. Les résultats mettent en evidence l'allumage et le développement de la flamme dans le domaine de non-équilibre, ainsi que le rapprochement à l'équilibre chimique local intérieur à la zone de hautes températures. Les réactions chimiques son pratiquemment éteintes aux deux cotés de la flamme même à de longues distances du bord avant de la plaque étant donné les basses températures présentes à ces endroits.

UNTERSUCHUNG EINER LAMINAREN DIFFUSIONSFLAMME IN EINER EBENEN PLATTENGRENZSCHICHT

Zusammenfassung—Es wird eine numerische Berechnung einer laminaren Wasserstoff-Sauerstoff-Diffusionsflamme in einer ebenen Plattengrenzschicht durchgeführt, um deren Flammenstruktur im Nichtgleichgewicht und in der Nähe des Gleichgewichts an verschiedenen Orten in der Grenzschicht zu untersuchen. In der Rechnung werden variable Stoffwerte einschließlich der Thermodiffusion und 15 Elementarreaktionen zwischen 8 Komponenten berücksichtigt. Die Ergebnisse zeigen die Zündung und die Entwicklung der Flamme im Nichtgleichgewicht sowie die Annäherung an das örtliche chemische Gleichgewicht innerhalb der Flammenzone. Auf beiden Seiten der Flammenzone sind die chemischen Reaktionen wegen der dort herrschenden niedrigen Temperaturen sogar in großen Abständen von der Vorderkante praktisch eingefroren.

АНАЛИЗ ДИФФУЗИОННОГО ПЛАМЕНИ В ЛАМИНАРНОМ ПОГРАНИЧНОМ СЛОЕ НА ПЛОСКОЙ ПЛАСТИНЕ

Аннотация — Выполнен численный расчет ламинарного водородно-кислородного диффузионного пламени в ламинарном пограничном слое на плоской пластине с целью выяснения его структуры в неравновесном и близком к равновесию состояниях в различных точках пограничного слоя. В расчетах использовались переменные характеристики, включая термодиффузию, и данные по 15 простым реакциям между 8 жидкостями. Приведены результаты по процессу воспламенения и развития неравновесного пламени и методика расчета локального химического равновесия внутри зоны пламени. Вследствие наличия низких температур с двух сторон зоны пламени химические реакции в них практически заморожены даже на достаточном удалении от передней кромки.